IOP Conference Series: Earth and Environmental Science

PAPER • **OPEN ACCESS**

An experimental study on air entrainment in a suction sump over critical-submergence condition

To cite this article: Akira Morita *et al* 2019 *IOP Conf. Ser.: Earth Environ. Sci.* **240** 032009

View the article online for updates and enhancements.

This content was downloaded from IP address 120.78.68.241 on 10/10/2019 at 10:04

IOP Conf. Series: Earth and Environmental Science **240** (2019) 032009 doi:10.1088/1755-1315/240/3/032009

An experimental study on air entrainment in a suction sump over critical-submergence condition

Akira Morita[1], **Katsuya Hirata**[1], **Masakatsu Hattori**[1], **Tsuyoshi Maeda**[1] **and Takashi Noguchi**[2]

[1] Department of Mechanical Engineering, Doshisha University, Kyoto 610-0321, Japan
[2] Department of Aeronautics and Astronautics, Kyoto University, Kyoto 615-8246, Japan

khirata@mail.doshisha.ac.jp

Abstract. In pump's sumps, the air entrainment sometimes occurs. In various industrial and environmental problems, the air entrainment often induces vibration, noise, low pumping efficiency or pump's collapse at the worst. The present aim is to understand the air entrainment appearing inside a simple and basic suction sump in the vertical-wet-pit-pump configuration. In particular, we focus upon the influences of governing parameters upon the occurrence-time ratio γ of the air entrainment, using a conductance-type electric sensor which can detect the existence of air bubbles through a suction pipe with no disturbances by the sensor probe and with a fine spatial resolution in order to achieve accurate measurements. As a result, we reveal the influences of the Froude number, the Reynolds number, the Weber number (or the Bond number) and three geometric parameters upon the air entrainment in over-critical-submergence condition.

1. Introduction

We deal with the flow into a suction pipe which is vertically inserted down into a suction sump across a mean free-water surface. This configuration is conventionally referred to as the "vertical wet-pit pump" or the "vertical-suspended wet-well pump," and has many practical advantages in construction, maintenance and operation. Most of the flows appearing in various industrial and environmental problems like the present suction-sump flow become often complicated owing to both of their unsteadiness with poor periodicity and their fully-three-dimensionality.

In power generation plants, irrigations, drainages and so on, the optimum designs of suction sumps have been needed to get low initial/running costs, compact scale, high efficiency and high performance. In recent years, we commonly require higher-level solutions to satisfy those needs. In such situations, the air entrainment into suction-pipe intakes becomes easy to occur, which often induces vibration, noise, low pumping efficiency or pump's collapse at the worst. Then, we should carefully design the suction sumps and suction pipes to prevent the air entrainment [1–5]. However, the air entrainment sometimes occurs even in many actual situations where operation is hard to prevent it.

As the air entrainment inside suction sumps is an important concern in practical aspects, there have been many researches about the air entrainment. Among such past studies, coherent dimensional-

Content from this work may be used under the terms of the Creative Commons Attribution 3.0 licence. Any further distribution of this work must maintain attribution to the author(s) and the title of the work, journal citation and DOI.
Published under licence by IOP Publishing Ltd

analysis approaches only concern the simplest geometry such as the "horizontal orifice," owing to the applicability of their systematic approaches to such a simple flow with less geometric parameters. However, actual suction sumps usually have more complicated geometries, due to broad-spectrum restrictions and requirements in practical aspects. And unfortunately, we have not enough knowledge even for the flow in a slightly-complicated-geometry suction sump such as a simple vertical-wet-pit-pump-configuration one. Concerning the vertical-wet-pit-pump configuration, we have carried out some studies [6–9], in addition to other researchers [10–15]. These studies suggest that we should know the flow and the air-entrainment mechanism more precisely, to prevent the air entrainment.

Our present purpose is to get accurate measurements of the air entrainment into a suction pipe in the vertical-wet-pit-pump configuration. Until now, we have usually judged the air-entrainment occurrence by means of a visually-based method (hereinafter, referred to as a visual method) [1–5]. This conventional visual method has been used prevailingly, because of its practicability and simplicity. However, because the visual method inherently means just the observation of free surfaces, we do not identify the air entrainment itself (will be described later). In our previous study [7], we developed a new and simple conductance-type electric bubble sensor, which can detect the existence of air bubbles through a suction pipe with no disturbances by sensor probes and with a fine spatial resolution. In the present study, we especially focus upon occurrence-time ratio γ of the air entrainment as well as Ref. [7] using the developed bubble sensor, not in the critical-submergence condition which is examined in Ref. [7] but in over-critical-submergence condition. Furthermore, we carry out the observation of free-surface pattern.

Nomenclature

B	Suction-sump breadth [m]
Bo	Bond number, $\equiv \rho w g D^2/\sigma = We^2/Fr^2$)
D	Outside diameter of a suction pipe [m]
d	Inside diameter of a suction pipe [m]
Fr	Froude number, $\equiv V_i/(gD)^{0.5}$
g	Gravitational acceleration [m/s^2]
H	Water level [m]
Q	(Volumetric) flow rate [m^3/s]
Re	Reynolds number, $\equiv V_i D/\nu$
S	Submergence [m]
S_c	Critical submergence [m]
t_0	Time [s]
V_i	Suction-pipe-intake velocity [m/s]
ν	Kinetic viscosity [m^2/s]
We	Weber number, $\equiv V_i(\rho_w D/\sigma)^{0.5}$
X	Back clearance [m]
Z	Bottom clearance [m]
γ	Occurrence-time ratio [-]
ρ_w	Water density [kg/m^3]
σ	Surface tension [N/m]
τ	Duration time [s]

2. Experimental method

2.1 Experimental apparatus

Figure 1 shows the present model, which is a simple system of a suction sump and a suction pipe in the vertical-wet-pit-pump configuration. D and d are the outer and inner diameters of the suction pipe,

respectively. A former is used as a characteristic length scale. The latter is fixed to $0.9D$. The suction-pipe intake has a bell-mouth shape.

The pipe is placed vertically on the centre line of the suction sump. B, X and Z denote the breadth of the suction sump, the clearance from the suction-pipe centre to the suction-sump back wall and the clearance between the suction-pipe intake and the suction-sump bottom wall, respectively. H is water level, namely, the height of a mean water-free surface, then the pipe's submergence depth S is equal to $(H - Z)$.

In order to specify model's dimensions, we define four non-dimensional geometric parameters; that is, a reduced sump breadth B/D, a reduced back clearance X/D, a reduced bottom clearance Z/D and a reduced submergence depth S/D.

The origin of the present coordinate system, the Cartesian coordinates x, y and z, is on the axis of the suction pipe and on the suction-sump bottom. The x axis is in the direction of the mainstream in the suction sump. The y axis is horizontal and perpendicular to the mainstream. And, the z axis is vertical.

In order to specify dynamical state, we define three non-dimensional kinetic parameters; that is, the Froude number Fr, the Reynolds number Re and the Weber number We. They are defined as follows.

$$Fr = V_{\mathrm{i}} / (gD)^{0.5} \tag{1}$$

$$Re = V_{\mathrm{i}} D / \nu \tag{2}$$

and

$$We = V_{\mathrm{i}} (\rho D / \sigma)^{0.5} \tag{3}$$

where g, ν, ρ and σ denote the gravitational acceleration, kinetic viscosity, fluid density and water-to-air surface tension, respectively. A characteristic velocity scale is the mean flow velocity V_{i} at the suction-pipe intake which is defined as

$$V_{\mathrm{i}} = 4\,Q / (\pi D^2) \tag{4}$$

where Q is the flow rate into the suction pipe. As a supplementary parameter, we use the Bond number such as

$$Bo = \rho g D^2 / \sigma \tag{5}$$

instead of We. When we define non-dimensional governing parameters, we can consider various options in the choice of characteristic scales. In the present study, we choose D and V_{i} as length and velocity scales, respectively (see Ref. [8] for the validity of these choices). In Table 1, we summarise the present values of experimental parameters. The range of them are determined to include practical or more severe condition.

The present experimental apparatus is similar with Ref. [8]. A turbo pump feeds working fluid (water) to a suction sump from a reservoir tank. We control the flow rate from another pump by a valve, and then control the water level in the suction sump. At the upstream of the suction sump, namely, at 0.84 m upstream from the back wall of the suction sump, we put a strainer to make flow uniform. The jet pump pumps up water from the suction sump into a suction pipe. We should note that the jet pump has less swirling component, than ordinary turbo pumps. The water from both the suction

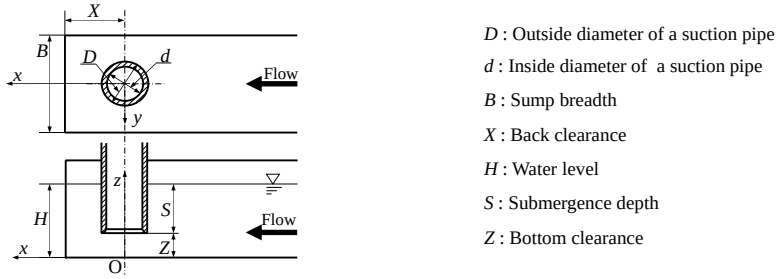

Figure 1. Model: suction sump and suction pipe in the vertical-wet-pit-pump configuration, together with coordinate system.

Table 1. Experimental parameters.

D [mm]	24 – 43
d [mm]	21 – 38
B/D	2.11 – 5.00
X/D	1.43 – 2.52
Z/D	0.26 – 1.43
S/D	0.2 – 2.5
Fr	1.2 – 2.8
Re (Re/Fr^2)	$2.8\times10^4 – 5.0\times10^4$ ($4.1\times10^3 – 2.2\times10^4$)
We (Bo)	19 – 25 (80 – 260)

pipe and the jet pump returns back into the reservoir. We measure the flow rate Q into the suction pipe from the suction sump using a triangle weir or a platform scale. To control surface tension, we add surfactant to water in some experiments (for the details, see Ref. [8]).

2.2 Free-surface patterns

Referring to previous studies[1, 3, 16–20] together with our preliminary observation, we have classified distinctive free-surface patterns in the suction sump into four types (a) – (d) [8] as shown in Figure 2. Then, the present classification is rather different from Ref. [2] (also see Ref. [8]). The free-surface pattern in the suction sump usually shifts from the type (a) to the type (d), as the submergence depth S decreases.

We should note that the above classification is quite conventional, being based on the visual observation of the free surfaces between air and water. Then, each type can be directly connected with neither the occurrence of the air entrainment nor the volume of the entrained air, in a strict sense.

The visual method is the most common method to judge the air-entrainment occurrence. However, due to ambiguous definitions of the air-entrainment occurrence, there has existed some confusion among researchers. (The main reason for the confusion, of course, comes from the lack of direct relations with the air entrainment itself.) Conventionally, the judgment of the air-entrainment occurrence by the visual method are given by the following manner, which is the same as Ref. [8]. When we observe any spatially-continuous air cores from a free surface to a suction-pipe intake, namely, any underwater air bulks accompanied with so-called “the fully-developed entraining vortices” even at a short instant, we recognise the air-entrainment occurrence (see Figure 2(c)). On the other hand, when we observe some spatially-intermittent air cores, namely, some underwater air bulks

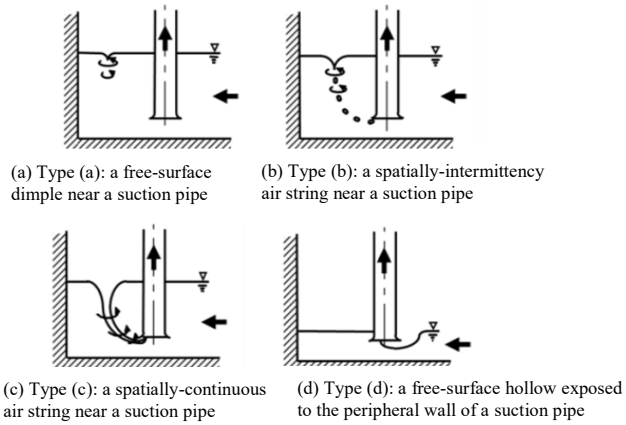

Figure 2. Types of distinctive free-surface patterns in suction sump [8].

accompanied with so-called "the intermittently-developed entraining vortices," we do not recognise the air-entrainment occurrence (see Figure 2(b)). In a strict sence, the critical submergence S_c is defined as the minimum value of S with the air entrainment. Then, the boundary between the types (b) and (c) should be at $S = S_c$. And, this is confirmed in our previous study [7].

Incidentally speaking, such a judgment manner is more objective and keeps a good reproductivity which has been confirmed in many preparatory experiments, although it lacks a thoroughly-theoretical background. (In fact, we have also confirmed that the results obtained with much longer sampling times than 300 sec almost coincide with the present results.) The present judgment manner is the same as Ref. [8]. Even if we use a somewhat-deferent judgment manner from the present one, the obtained results are considered to be qualitatively identical with the present results (also see Ref. [8]).

2.3 Definition of occurrence-time ratio γ

For an accurate detection of the air entrainment into the suction pipe, we developed a bubble sensor (for the details, see Ref. [7]). The bubble sensor utilises the same principle as the conductance-type void-ratio meters. By the bubble sensor, we can instantaneously know the occurrence of the air entrainment.

We usually record the output voltage from the bubble sensor for 300 sec in each case. Using this raw time-series data, we calculate an occurrence-time ratio γ which represents the ratio of the air-entrainment-occurrence time to the total recording time. Its definition is given by

$$\gamma = \frac{\sum_{i=1}^{n} \tau_i}{t_0}, \tag{6}$$

where t_0 denotes the total recording time which is equal to 300 sec. And, n denotes the total number of the air-entrainment occurrence for $t = 0 - t_0$. During a duration time τ_i, the i-th air entrainment occurs. The air entrainment occurs at any time during the total recording time, when $\gamma = 1$. And, the air entrainment never occur, when $\gamma = 0$. Supplementarily speaking, one main reason why we consider γ is that the concerned phenomenon has a very-weak periodicity, and that γ tends to have a constant value for enough large t_0.

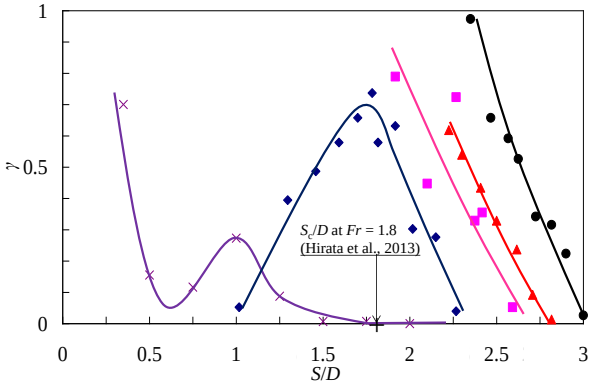

Figure 3. Air-entrainment occurrence-time ratio γ against reduced submergence depth S/D.
×; $B/D = 3.15$, $X/D = 1.71$, $Z/D = 0.71$, $Fr = 1.8$, $Re = 3.2\times10^4$ ($Re/Fr^2 = 9.9\times10^3$) and $We = 21$ ($Bo = 140$).
◆; $B/D = 10$, $X/D = 4$, $Z/D = 3$, $Fr = 1.0$ and $Re = 3.2\times10^4$ [21].
■; $B/D = 10$, $X/D = 4$, $Z/D = 3$, $Fr = 1.5$ and $Re = 4.8\times10^4$ [21].
▲; $B/D = 10$, $X/D = 4$, $Z/D = 3$, $Fr = 1.9$ and $Re = 6.4\times10^4$ [21].
●; $B/D = 10$, $X/D = 4$, $Z/D = 3$, $Fr = 2.2$ and $Re = 7.2\times10^4$ [21].
+; $S_c/D = 1.6\times Fr^{2/5}$, $B/D = 3.57$, $X/D = 2.11$, $Z/D = 0.71$, $Re = 3.8\times10^4 > 3.0\times10^4$ ($Re/Fr^2 = 1.2\times10^4 > 8.0\times10^3$) and $We = 20 - 26 > 12$ ($Bo = 105 - 309 > 95$) [8]

Furthermore, we carry out the observation of free-surface pattern, together with the above bobble-sensor measurement.

3. Results and Discussion

3.1 Influence of reduced submergence depth S/D upon γ

As mentioned in 2.2, we now consider seven governing parameters such as B/D, X/D, Z/D, S/D, Fr, Re and We. Among the seven parameters, we regard S/D as a primary parameter as well as Iversen [16] and Denny [17]. Actually, the influence of S/D upon γ is qualitatively common in many cases, and the corresponding free-surface pattern is as well in many cases. (This will be shown later.) Then, we hereinafter investigate the influence of S/D upon γ at first. Next, we investigate the influences of the other parameters upon the relation between S/D and γ.

Figure 3 shows a typical example of the relation between S/D and γ together with the free-surface-pattern type, namely, the occurrence-time ratio γ plotted against the reduced submergence depth S/D, together with another research [21]. In addition, the Figure also shows the critical value S_c/D of the reduced submergence depth obtained in our previous study [8].

As S/D decreases from 2.0 to 1.0, γ monotonically increases. On the other hand, as S/D decreases from 1.0 to 0.7, γ monotonically decreases. Then, γ attains the maximum at $S/D \simeq 1.0$. At $S/D < 0.7$, γ progressively increases with decreasing S/D. Then, at $S/D \simeq 0.7$, γ attains the minimum which is close to zero. We can also observe shifts of free-surface pattern from the type (a) to the type (d), corresponding to the above behaviour of γ with decreasing S/D. Specifically speaking, the type (a) or (b) appears in a range of $S/D > 1.8$. The type (c) appears in a range of $S/D = 0.7 – 1.8$. Therefore, the critical submergence depth S_c/D in reduced form becomes about 1.8 between types (b) and (c), which consides with [8]. At $S/D < 0.7$, the type (d) appears, instead of the type (c). Then at $S/D \simeq 0.7$, there exists a free-surface-pattern shift between the types (c) and (d). Both the above relation between S/D and γ and the above relation between S/D and free-surface pattern become bases, when we will discuss the influences of the other parameters than S/D in the following subsection.

Both the above relations are qualitatively the identical as Iversen [16] and Denny [17] and as Okamoto et al. [21] at $S/D > 1.0$. From a quantitative point of view, the discrepancies of γ between the present study and previous ones could be due to different governing parameters in addition to different measuring methods of γ.

3.2 Influences of the other governing parameters

In this subsection, we discuss the influences of the other parameters than S/D, on the basis of the relation between S/D and γ together with the relation between S/D and free-surface pattern. At first, we will reveal the influences of three kinetic parameters Fr, Re and We. Then, we will reveal those of three geometric parameters B/D, X/D and Z/D. In the former, we fix the values of the three geometric parameters such as $B/D = 3.15$, $X/D = 1.71$ and $Z/D = 0.71$, where the air entrainment is easy to occur. In the latter, we fix the values of the three kinetic parameters such as $Fr = 1.8$, $Re = 3.2\times10^4$ and $We = 21$ (or $Bo = 140$), where we expect that the influences of Re and We (or Bo) are negligible according to our previous study [8] on the critical submergence. Actually in this report, we show only the influence of We as an example of the former, and only the influence of B/D as an example of the latter, due to the limitation of paper's volume.

3.2.1 Influence of Weber number We (or Bond number Bo)

We now fix the values of B/D, X/D, Z/D, Fr and Re, and compare the results at different two values of We (or Bo). Figure 4 shows We effect (or Bo effect) upon γ, namely, γ plotted against S/D, together

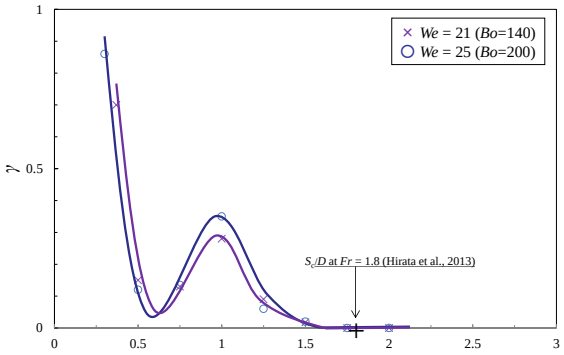

(a) At $Fr = 1.8$.

×; $B/D = 3.15$, $X/D = 1.71$, $Z/D = 0.71$, $Fr = 1.8$, $Re = 3.2\times10^4$ ($Re/Fr^2 = 9.9\times10^3$) and $We = 21$ ($Bo = 140$).
○; $B/D = 3.15$, $X/D = 1.71$, $Z/D = 0.71$, $Fr = 1.8$, $Re = 3.2\times10^4$ ($Re/Fr^2 = 9.9\times10^3$) and $We = 25$ ($Bo = 200$).
＋; $S_c/D = 1.6\times Fr^{2/5}$, $B/D = 3.57$, $X/D = 2.11$, $Z/D = 0.71$, $Re = 3.8\times10^4 > 3.0\times10^4$ ($Re/Fr^2 = 1.2\times10^4 > 8.0\times10^3$) and $We = 20 - 26 > 12$ ($Bo = 105 - 309 > 95$) [8].

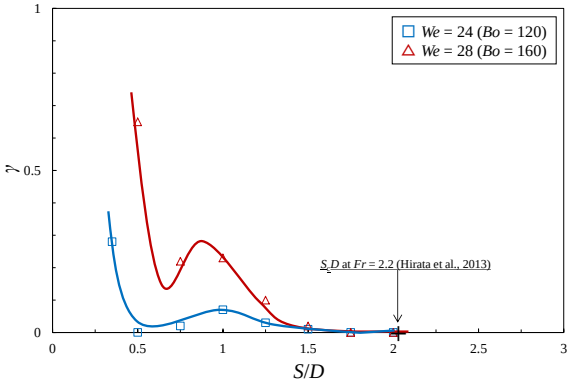

(b) At $Fr = 2.2$.

□; $B/D = 3.15$, $X/D = 1.71$, $Z/D = 0.71$, $Fr = 2.2$, $Re = 3.2\times10^4$ ($Re/Fr^2 = 6.6\times10^3$) and $We = 24$ ($Bo = 120$).
△; $B/D = 3.15$, $X/D = 1.71$, $Z/D = 0.71$, $Fr = 2.2$, $Re = 3.2\times10^4$ ($Re/Fr^2 = 6.6\times10^3$) and $We = 28$ ($Bo = 160$).
＋; $S_c/D = 1.6 \times Fr^{2/5}$, $B/D = 3.57$, $X/D = 2.11$, $Z/D = 0.71$, $Re = 3.8\times10^4 > 3.0\times10^4$ ($Re/Fr^2 = 7.9\times10^3 > 8.0\times10^3$) and $We = 20 - 26 > 12$ ($Bo = 105 - 309 > 95$) [8].

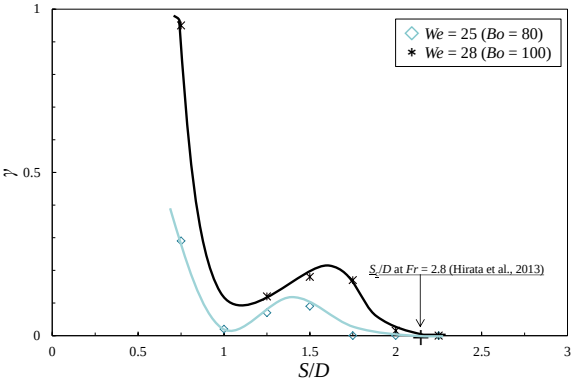

(c) At $Fr = 2.8$.

◇; $B/D = 3.15$, $X/D = 1.71$, $Z/D = 0.71$, $Fr = 2.8$, $Re = 3.2\times10^4$ ($Re/Fr^2 = 4.1\times10^3$) and $We = 25$ ($Bo = 80$).
＊; $B/D = 3.15$, $X/D = 1.71$, $Z/D = 0.71$, $Fr = 2.8$, $Re = 3.2\times10^4$ ($Re/Fr^2 = 4.1\times10^3$) and $We = 28$ ($Bo = 100$).
＋; $S_c/D = 1.6 \times Fr^{2/5}$, $B/D = 3.57$, $X/D = 2.11$, $Z/D = 0.71$, $Re = 3.8\times10^4 > 3.0\times10^4$ ($Re/Fr^2 = 4.8\times10^3 > 8.0\times10^3$) and $We = 20 - 26 > 12$ ($Bo = 105 - 309 > 95$) [8].

Figure 4. *We* effect (or *Bo* effect) on air-entrainment occurrence-time ratio γ.

with the S_c/D obtained in our previous study [8]. Figures (a), (b) and (c) represent the results at Fr = 1.8, 2.2 and 2.8, respectively.

At, first, we see Figure 4(a). The result at We = 21 (or Bo = 140) is the same as that in Figure 3. The result at We = 25 (or Bo = 200) almost coincides with that at We = 21, from both qualitative and quantitative view points. Furthermore, we can confirm that the corresponding free-surface patterns at We = 25 are the same as those at We = 21. As a result, the influences of We (or Bo) upon γ and upon flow pattern are negligible at We > 21 (or Bo > 140) even at $S/D < S_c/D$. This result is consistent with our previous study [8] where S_c/D is independent of both We and Re at We > 12 (or Bo > 95) and $Re > 3.0\times10^4$ (or $Re/Fr^2 > 8.0\times10^3$).

Second, we see Figure 4(b). The result at We = 24 (or Bo = 120) is similar with that at We = 28 (or Bo = 160). In addition, the corresponding free-surface patterns at We = 24 are the same as those at We = 28. However from a quantitative point of view, we can see a clear difference between both the results. In other words, with decreasing We, γ tends to decreases, then the air entrainment tends to be prevented. This tendency is acceptable, when we remind that surface tension becomes strong with decreasing We (or Bo). Besides, we can see another clear difference. That is, the values of S/D where γ attains the maximum/minimum depends upon We (or Bo).

Finally, we see Figure 4(c). Again, the result at We = 25 (or Bo = 80) is similar with that at We = 28 (or Bo = 100). In addition, the free-surface flow patterns at We = 25 are the same as those at We = 28. However from a quantitative point of view, we can see the two clear differences between both the results, as well as Figure 4(b).

In summary, we can ignore the influences of We (or Bo) at $Fr \lesssim 2$. On the other hand, we cannot ignore the influences at $Fr \gtrsim 2$, even at We > 12 (or Bo > 95) where we can ignore the influences upon S_c/D. More specifically, the influences indicate both such a tendency as γ decrease with decreasing We (or Bo) and such a dependency as both the values of S/D with the maximum/minimum γ's are the function of We (or Bo). In addition, we cannot recognise both the influences at $Bo \gtrsim 140$ even at $S/D < S_c/D$. Then, we can ignore the influences at $Bo \gtrsim 140$. On the other hand, we cannot find out such a simple criterion on We as that on Bo, from Figure 4.

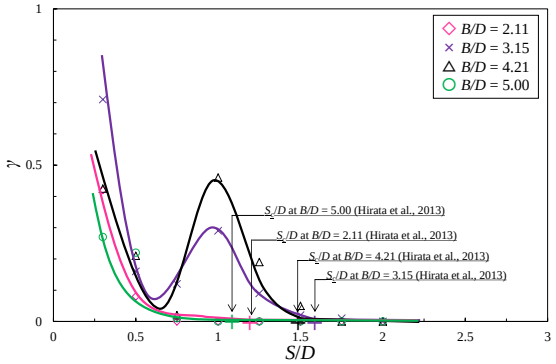

Figure 5. B/D effect on air-entrainment occurrence-time ratio γ.
◇; B/D = 2.11, X/D = 1.71, Z/D = 0.71, Fr = 1.8, $Re = 3.2\times10^4$ ($Re/Fr^2 = 9.9\times10^3$) and We = 21 (Bo = 140).
×; B/D = 3.15, X/D = 1.71, Z/D = 0.71, Fr = 1.8, $Re = 3.2\times10^4$ ($Re/Fr^2 = 9.9\times10^3$) and We = 21 (Bo = 140).
△; B/D = 4.21, X/D = 1.71, Z/D = 0.71, Fr = 1.8, $Re = 3.2\times10^4$ ($Re/Fr^2 = 9.9\times10^3$) and We = 21 (Bo = 140).
○; B/D = 5.00, X/D = 1.71, Z/D = 0.71, Fr = 1.8, $Re = 3.2\times10^4$ ($Re/Fr^2 = 9.9\times10^3$) and We = 21 (Bo = 140).
+; B/D = 2.11, X/D = 1.32, Z/D = 0.71, Fr = 1.6, $Re = 3.8\times10^4$ ($Re/Fr^2 = 1.5\times10^4$) and We = 22.4 (Bo = 197) [8].
+; B/D = 3.15, X/D = 1.32, Z/D = 0.71, Fr = 1.6, $Re = 3.8\times10^4$ ($Re/Fr^2 = 1.5\times10^4$) and We = 22.4 (Bo = 197) [8].
+; B/D = 4.21, X/D = 1.32, Z/D = 0.71, Fr = 1.6, $Re = 3.8\times10^4$ ($Re/Fr^2 = 1.5\times10^4$) and We = 22.4 (Bo = 197) [8].
+; B/D = 5.00, X/D = 1.32, Z/D = 0.71, Fr = 1.6, $Re = 3.8\times10^4$ ($Re/Fr^2 = 1.5\times10^4$) and We = 22.4 (Bo = 197) [8].

3.2.2 Influence of reduced sump breadth B/D

We now fix the values of X/D, Z/D, Fr, Re and We (or Bo), and compare the results at different four values of B/D. Figure 7 shows B/D effect upon γ, namely, γ plotted against S/D at four values of B/D, together with S_c/D obtained in our previous study [8]. The result at $B/D = 3.15$ is the same as Figure 3.

From a qualitative point of view, both the behaviour of γ with decreasing S/D at $B/D = 2.11$ and the corresponding free-surface pattern are different from Figure 3. More specifically, as S/D decreases, γ at $B/D = 2.11$ monotonically increases without the maximum/minimum. About the corresponding free-surface pattern at $B/D = 2.11$, the type (d) becomes easy to appear in a wide range of S/D at $S/D < S_c/D$, while the type (c) is difficult to be observed at $S/D < S_c/D$. Both at $B/D = 4.21$ are the same as those at $B/D = 3.15$. Again, both at $B/D = 5.00$ are the same as those at $B/D = 2.11$.

From a quantitative point of view, γ at $S/D \simeq 1.0$ is remarkable large at $B/D = 3.15$ and 4.21. Corresponding to this, S_c/D's at $B/D = 3.15$ and 4.21 are much larger than those at $B/D = 2.11$ and 5.00. The flow pattern at $S/D \simeq 1.0$ is in the type (c) at $B/D = 3.15$ and 4.21. And, the flow pattern at $S/D < S_c/D$ is almost in the type (d) at $B/D = 2.11$ and 5.00. In summary, such a condition as $B/D \simeq$ 3–4 is suitable for the type (c). Then, γ at $B/D \simeq$ 3–4 tends to become remarkably large at $S/D \simeq 1.0$, with enhancing the air entrainment. This condition is linked to the increase of S_c/D.

4 Conclusions

In order to understand the air entrainment appearing inside a simple and basic suction sump in the vertical-wet-pit-pump configuration, we have focused on the influences of governing parameters upon the occurrence-time ratio γ of the air entrainment, using a conductance-type electric sensor which can detect the existence of air bubbles through a suction pipe with no disturbances by the sensor probe and with a fine spatial resolution in order to achieve accurate measurements. As a result, we have revealed the influences of the Weber number (or the Bond number) as an examples of three kinetic parameters like the Froude number, the Reynolds number and We and a reduced sump breadth B/D as an example of three geometric parameters like B/D, a reduced back clearance X/D and a reduced bottom clearance Z/D upon the air entrainment in such an over-critical-submergence condition as $S/D < S_c/D$.

About the influence of Weber number We (or Bond number Bo), we can ignore the influences of We (or Bo) at $Fr \lesssim 2$. On the other hand, we cannot ignore the influences of We (or Bo) at $Fr \gtrsim 2$, even at $We > 12$ (or $Bo > 95$) where we can ignore the influences of We (or Bo) upon S_c/D. More specifically, As S/D decreases from S_c/D to about 1.0, γ monotonically increases. On the other hand, as S/D decreases from about 1.0 to about 0.5, γ monotonically decreases. At $S/D <$ about 0.5, γ progressively increases with decreasing S/D. Then, γ attains the maximum at $S/D \simeq 1.0$ and the minimum at $S/D \simeq$ 0.5. The free-surface pattern shifts from the type (a) to the type (d), corresponding to the above behaviour of γ with decreasing S/D. Quantitatively, the influences of We (or Bo) indicate both such a tendency as γ decrease with decreasing We (or Bo) and such a dependency as both the values of S/D with the maximum/minimum γ's are the function of We (or Bo).

About the influence of reduced sump breadth B/D, such a condition as $B/D \simeq$ 3–4 is suitable for the type (c). Then, γ at $B/D \simeq$ 3–4 tends to become remarkably large at $S/D \simeq 1.0$.

References

[1] Toyokura T et al. 1984 *Standard method for model testing the performance of a pump sump JSME Standard JSME S 004* JSME Tokyo (in Japanese)
[2] Claxton J et al. 1998 *American national standard for pump intake design (the 1988 HI Standard) ANSI/HI9.8-1998* Hydralic Institute Parsippany New Jersey USA
[3] Kamemoto K et al. 2005 *Standard method for model testing the performance of a pump sump TSJ Standard TSJ S 002* TSJ Tokyo (in Japanese)
[4] Matsui J and Kawane H 2009 Outline on pump sump and its model test *Turbomachinery* **37**

No. 1 4–11 (in Japanese)
[5] Zhao L 2009 Visualization of vortices in pump sump *Journal of the Visualization Society of Japan* **30** No. 116 28–33 (in Japanese)
[6] Funaki J Neya M Hattori M Tanigawa H. and Hirata K 2008 Flow measurements in a suction sump by UVP *Journal of Fluid Science and Technology JSME* **3** No. 1 68–79
[7] Hirata K Saitoh K Hattori M Nakatani Y and Funaki J 2009 Occurrence-time-ratio measurements on air entrainment in a suction sump *Journal of Fluid Science and Technology JSME* **4** No. 1 47–61
[8] Hirata K Funaki J Kubota Y Inagaki K Taoka M and Saida T 2013 Occurrence condition of air entrainment into a vertical wet-pit pump *Journal of Fluid Science and Technology JSME* **8** No. 3 364–79
[9] Hirata K Shintani A Kawaguchi R Inagaki K Nagura T and Maeda T 2016 3D-PTV measurement verified by UVP for unsteady and three-dimensional flow inside a suction sump *Journal of Fluid Science and Technology JSME* **11** No. 3 1–13
[10] Oshima M and Tagomori M 1992 On critical dimensions for air-entraining vortices of a suction sump *Turbomachinery* **20** No. 4 205–10 (in Japanese)
[11] Kuwakino S 1993 On the prevention against air-entraining vortices in a suction sump *Turbomachinery* **21** No. 6 343–49 (in Japanese)
[12] Nagahara T Sato T Kawabata S and Okamura T 2002 Effect of the submerged vortex cavitation in pump suction intake on mixed flow pump impeller *Turbomachinery* **30** No. 2 70–75 (in Japanese)
[13] Zhao L and Nohmi M 2011 Numerical prediction of air-entrained vortex in pump sump using VOF method *Turbomachinery* **39** No. 7 425–30 (in Japanese)
[14] Kanemori Y and Pan Y 2015 Surface vortex prediction and preventing technique in pump intake sump *Turbomachinery* **43** No. 2 90–98 (in Japanese)
[15] Yamasaki R Kouchi T Nagata Y and Yanase S 2017 OpenFOAM analysis of air-entraining and submerged vortices in pump sump *Trans.of the JSME* **83** No. 853 1–13 (in Japanese)
[16] Iversen H W 1953 Studies of submergence requirements of high-specific-speed pump *Trans. of ASME* **75** 635–41
[17] Denny D F 1956 An experimental study of air-entraining vortices in pump sumps *Proc. IMechE* **170** No. 2 106–16
[18] Prosser M J 1977 *The hydraulic design of pump sumps and intakes* BHRA Cranfield Bedford UK
[19] Rajagopal H Y 1981 Prevention of vortices at pump intakes *Power Engineering* January 52–55
[20] Padmanabhan M and Hecker G E 1984 Scale effects in pump sump models *Journal of Hydraulic Engineering ASCE* **110** No. 11 1540–56
[21] Okamoto H Kamemoto K and Nakaguchi I 1991 Intermittency of the air entraining vortex and the submerged vortex in a suction sump *Trans. of JSME Series B* **57** No. 536 1210–13 (in Japanese)